Geomechanics and Engineering, *Vol. 42, No. 3 (2025) 221-228*
https://doi.org/10.12989/gae.2025.42.3.221

Numerical analysis using a newly developed 3D finite element procedure - Part II: Stress behavior for local loading

Seong-Kyu Yun[a], Hyeonsu Yun[b] and Gichun Kang*

Department of Civil Engineering, College of Engineering, Gyeongsang National University, 501 Jinjudae-ro, Jinju, Gyeongsangna,-do 52828, Republic of Korea

(*Received October 13, 2024, Revised July 8, 2025, Accepted July 9, 2025*)

Abstract. A number of artificial islands have been created in Osaka. These reclaimed islands have undergone much difficulty in the ground behavior due to unforeseen occurrence. These problems are caused by the following special features of the seabed in Osaka Bay. The modeling of permeability of the Pleistocene sand layer is not easy. And the Pleistocene clays deposited are so-called "quasi-overconsolidated clays". Most of all, one and two dimensional approaches have a limitation in assessing the stress and deformation due to reclamation. Because the seabed was observed non-homogeneity and irregular thickness. For the above mentioned reasons, the Author developed 3D FEM program using the elasto-viscoplastic constitutive model. And this developed 3D program has been validated and demonstrated by comparison with existing 2D studies. In this paper, stress and deformation analyses of the Pleistocene foundations for group pile supported elevated bridges were conducted with the developed 3D elasto-viscoplastic finite element code. The calculated performance showed a serious reduction in stress increment with depth, even at the center of the group piles. As far as the deformation is concerned, a compressive deformation naturally took place associated with the lateral expansion caused by the loading at the group pile.

Keywords: elasto-viscoplastic constitutive model; local loading; reclaimed marine foundation; stress dispersion; three-dimensional(3D) analysis

1. Introduction

In Japan, a number of large-scale reclamations have been executed in Osaka Bay in past decades, including Kansai International Airport, Port Island, and Rokko Island (Fig. 1). The large-scale offshore reclamation has undergone unexpectedly large and long-term ground behavior. The sea-bed deposits of Osaka Bay have been formed due to the soil supplied from the rivers on the sinking base (Kobayashi *et al.* 2001). In Osaka Bay, the sedimentary deposits consist of the Holocene clay underlain by the alternating Pleistocene clay and sand gravel deposits rising and falling sea levels due to historical ice ages. It is difficult to predict the ground behavior, which is a large landfill Island located in Osaka Bay.

The Pleistocene clays have a distinct structure due to the long-term effect of diagenesis. The Pleistocene clays in Osaka Bay exhibited slight overconsolidation with an OCR of 1.2 to 1.6 on average, although they are geologically normally consolidated. Therefore, the Pleistocene clay deposited in Osaka Bay is a so called "quasi-overconsolidated clay" without definite mechanical overconsolidation process. Mimura and Jang (2004) proposed the concept of compression in which viscoplastic behavior is assumed to occur even in the quasi-overconsolidated region less than pc for the Pleistocene clays in Osaka Bay. On the basis of the data from elastic wave exploration and in-site boring logs, Ito *et al*. (2001) summarized that the Pleistocene sand gravel deposits are not always distributed uniformly in thickness, continuously and that not a small amount of fine contents is included in them. The most serious problem originating from these sand gravel deposits is "permeability", that controls the rate of consolidation of sandwiched Pleistocene clays because the net values of the coefficient of permeability based on laboratory experiments do not necessarily function as representatives for such non-uniform sand gravel layers with occasional horizontal discontinuity and/or variation of thickness. The concept of "mass permeability" for the sandwiched Pleistocene sand gravel layers was introduced by Mimura and Jeon (2011, 2013), Jeon and Mimura (2011), Jeon (2012).

On the basis of the above-mentioned concept, a series of elasto-viscoplastic finite element analyses were performed to assess the long-term deformation of the alternating Pleistocene foundation through the 2D finite element analysis. 2D analyses are generally used when one of the representative cross-sections satisfies the phenomenon of the entire cross-section, but the distribution of the foundation in Osaka Bay was observed as non-homogeneous with irregular thickness through the geophysical exploration. Therefore, three-dimensional consolidation analysis is required. Not only in Osaka Bay,

*Corresponding author, Associate Professor
E-mail: gkang@gnu.ac.kr
[a]Research Professor
E-mail: tjdrb330@gnu.ac.kr
[b]Ph.D. Candidate
E-mail: gustn0672@gnu.ac.kr

ISSN: 2005-307X (Print), 2092-6219 (Online)

Fig. 1 Location map and plan view of Osaka Bay (Osaka Bay 2009).

but also in various fields of geotechnical engineering, the need for three-dimensional analysis has increased, leading to numerous studies on this topic (Yamaguchi *et al.* 2018, Yang and Liu 2018, Song and Tian 2019, Nawel and Salah 2015, Sun *et al*. 2018).

For the above-mentioned reasons, Yun (2020) developed a three-dimensional finite element analysis program using the elasto-viscoplastic constitutive model. And this developed three-dimensional program has been validated and demonstrated by comparison with existing two-dimensional studies.

In this paper, stress and deformation analyses of the Pleistocene foundations loaded by base local loading of the group pile supported elevated bridge were conducted with the developed three-dimensional elasto-viscoplastic finite element code. The calculated performance showed a significant reduction in stress increment with depth, even at the center of the group piles. As far as the deformation is concerned, a compressive deformation naturally occurred associated with the lateral expansion caused by the loading of the group pile.

2. Framework of numerical assessment

2.1 Elasto-viscoplastic model

The elasto-viscoplastic constitutive model proposed by Sekiguchi (1977) was used in newly developed 3D program. In general, the viscoplastic flow rule (Eq. (1)) is as follows.

$$\dot{\varepsilon}_{ij}^{p} = \Lambda \frac{\partial F}{\partial \sigma_{ij}^{'}} \tag{1}$$

in which,

F=Viscoplastic potential

Λ= Proportional constant

Viscoplastic potential F is shown in Eq. (2).

$$F = \alpha \cdot ln\left[1 + \frac{\dot{v}_0 \cdot t}{\alpha} exp\left(\frac{f}{\alpha}\right)\right] = v^{p} \tag{2}$$

in which,

α= Secondary compression index

$\dot{v_o}$ =Volumetric strain rate

f =Function in terms of the effective stress

v^p=Viscoplastic volumetric strain

The concrete form of the model is shown in Eq. (3). The resulting constitutive relations are implemented into the finite element analysis procedure through the following incremental form (Mimura and Sekiguchi 1986).

$$\{\Delta\sigma^{'}\} = [D^{evp}]\{\Delta\varepsilon\} - \{\Delta\sigma^{R}\} \tag{3}$$

in which,

$\{\Delta\sigma^{'}\}$= Effective stress increments

$\{\Delta\varepsilon\}$= Strain increments

$[D^{evp}]$= Elasto- viscoplastic stiffness matrix

$\{\Delta\sigma^{R}\}$= Relaxation stress

Relaxation stress is the increase in stress over time when the strain rate remains constant. The pore water flow is assumed to obey isotropic Darcy's law. It is assumed that the coefficient of permeability, k, depends on the void ratio, e, in the expressing Eq. (4).

$$k = k_0 \cdot exp\left(\frac{e - e_0}{\lambda_k}\right) \tag{4}$$

In, which,

k_o= Initial value of k at $e = e_o$

λ_k= Material constant

Material constant, λ_k, controls the rate of change in permeability subjected to a change in the void ratio. Note that each quadrilateral element consists of four constant strain triangles, and the nodal displacement increments and the element pore water pressure are taken as the primary unknowns of the problem. The finite element equations governing those unknowns are established on the basis of Biot's formulation (Christian 1968, Akai and Tamura 1976), and are solved numerically using the semi-band Gaussian elimination method.

2.2 Conditions of analysis

Stress and deformation analyses of the Pleistocene foundations for a group pile supported elevated bridge is conducted with the developed three-dimensional elasto-viscoplastic finite element program. The foundation model and soil parameter for numerical analysis were determined based on representative boring points of Osaka Bay. As shown in Fig. 2, Piles are installed up to -56 m with a supporting Pleistocene sand gravel layer for pier installation. This analysis predicts the behavior of the foundation for Pleistocene clay layers due to the additional load of the elevated bridge structure. Therefore, the sand and clay layers were modeled from -56 m, to which the load was applied. The load was applied to 11 * 17m of the bridge pier area. Considering the load of the superstructure, the total load was applied as 68400kN. The size of the model was designed to be large enough not to be affected by the loading. The real foundation model for numerical is shown in Figs. 3 and 4 appears as the schematic of the foundation model for numerical analysis, an expansion of Fig. 3 for clearer view. The total number of elements is 3315, and the

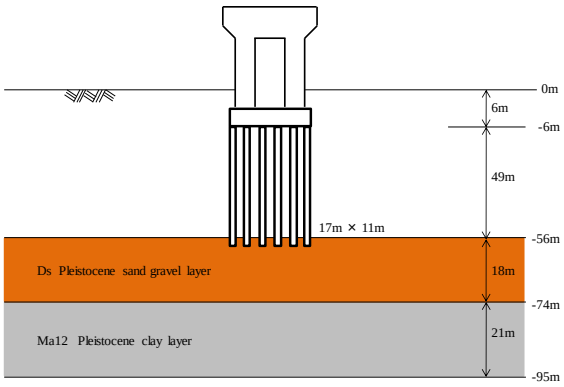

Fig. 2 Outline of numerical analysis

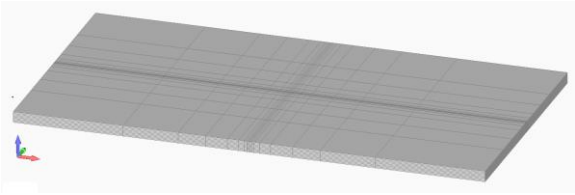

Fig. 3 Real foundation model for numerical analysis

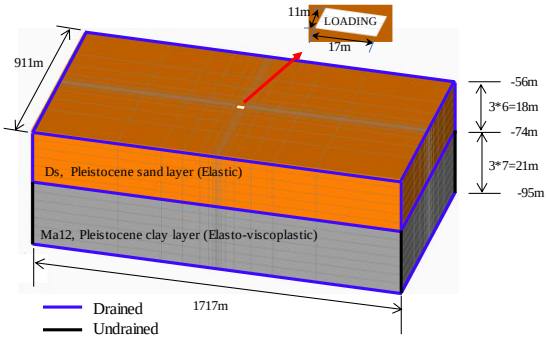

Fig. 4 Schematic of foundation model for numerical analysis

total number of nodes is 4032. The lateral boundary of the clay layers is assumed to be undrained, while that of the sand layers is assumed to be fully drained. The bottom boundary is hence assumed to be drained.

The soil parameters of both sand and clay layers were summarized in Tables 1 and 2. These parameters were determined from representative values of Pleistocene sand (Ds) and clay (Ma12) layers in Osaka Bay.

3. Results and discussions

3.1 Performance of excess pore water pressurel

The calculated distribution of excess pore water pressure with depth is shown in Fig. 5. The pile loading is applied instantaneously for the stable analysis without considering the actual construction sequence. As a result, the maximum excess pore water pressure occurred after 5 days from the loading. Dissipation of excess pore water pressure was

Table 1 Soil parameters for the Pleistocene sand gravel layers

E (kPa)	1.00e+4
k_0 (m/s)	2.16e+1
K_0	0.5
ν	0.33
γt (t/m3)	1.0

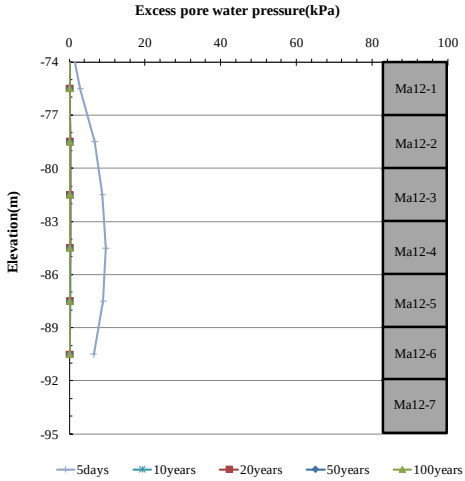

Fig. 5 Calculated distribution of excess pore water pressure with depth

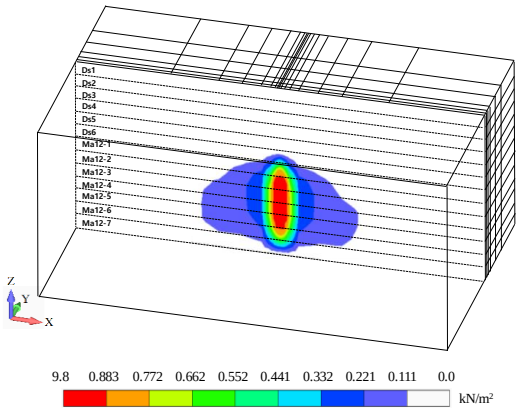

Fig. 6 Excess pore water pressure in the ground in three dimensions for after 5days

almost completed in all sand layers except the Ds6 layer. In the case of the clay layer, the maximum excess pore water pressure was generated from the Ma 12-4 layer in the middle layer, and the excess pore water pressure decreased more and more in the vertical and horizontal directions. Fig. 6 shows the excess pore pressure in the ground in three dimensions after 5 days. This Figure is a cut of Fig. 4 in the y direction.

3.2 Performance of stress and strain

Stress and deformation analyses of the Pleistocene foundations for a group pile supported elevated bridge is

Table 2 Soil parameters for the Pleistocene clay layers

	Ma12-1	Ma12-2	Ma12-3	Ma12-4	Ma12-5	Ma12-6	Ma12-7
e_0	1.243	1.559	1.671	1.745	1.706	1.753	1.808
Λ	0.2821	0.4817	0.4830	0.5859	0.5560	0.6410	0.6605
K	0.0282	0.0481	0.0483	0.0586	0.0556	0.0641	0.0661
G_0 (kPa)	1533.8202	1053.5967	1123.9635	974.5097	1009.2952	910.0174	919.6494
k_0 (m/s)	1.39e-4	2.08e-4	2.00e-4	2.36e-4	2.27e-4	2.57e-4	2.60e-4
KOC	0.5926	0.5926	0.5926	0.5926	0.6042	0.6042	0.6042
γ_s (t/m3)	0.738	0.638	0.608	0.591	0.594	0.582	0.572
M	1.3	1.3	1.3	1.3	1.25	1.25	1.25
α	0.006288	0.009413	0.009042	0.010672	0.010273	0.011642	0.011762
ν	0.3594	0.3594	0.3594	0.3594	0.3639	0.3639	0.3639
v_0 (day-1)	6.390e-07	9.564e-07	9.188e-07	1.084e-06	1.044e-06	1.183e-06	1.195e-06
λk	0.2821	0.4817	0.4830	0.5859	0.5560	0.6410	0.6605
OCR	1.2	1.2	1.2	1.2	1.2	1.2	1.2
K_0	0.5611	0.5611	0.5611	0.5611	0.5720	0.5720	0.5720
λ_{OC}	0.02821	0.04817	0.04830	0.05859	0.05560	0.06410	0.06605
κ_{OC}	0.002821	0.004817	0.004830	0.005859	0.005560	0.006410	0.006605
p_c (kPa)	862.2637	886.5611	908.5630	929.7349	950.6596	971.4254	991.8028

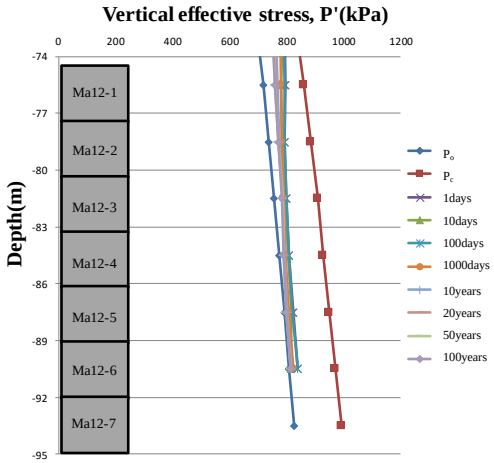

Fig. 7 Vertical effective stress condition with depth

conducted with the developed three-dimensional elasto-viscoplastic finite element program. The foundation model and soil parameter for numerical analysis was determined based on representative boring points of Osaka Bay.

The vertical effective stress condition with depth is shown in Fig. 7. Here, p_o denotes the initial vertical effective stress, and p_c is the consolidation yield stress and others denote the effective vertical stress of each time. The effective stresses still remain below p_c for the Pleistocene clay layers. Pleistocene clay layers behave as quasi-overconsolidated during the analysis time. It is true that the vertical effective stress at all Pleistocene layers is steadily dissipated in time.

Fig. 8 shows the calculated contours of vertical effective stress for the sand layer in three dimensions. Fig. 8(a) indicates calculated contours of vertical effective stress in all sand layers. Fig. 8(c) is a cut of Fig. 8(a) in the y direction, and Figs. 8(b) and 8(d) are enlargement of the center of Figs. 8(a) and 8(c), respectively. The newly developed three-dimensional program made it easy to see the distribution of calculated contours of effective stress in the sand layers, as shown in these Figs.

Figs. 9(a)-9(c) show the time-effective stress relation and the time-strain relation for a center element of the sand layer (Ds1). Fig. 9(a) is related to vertical effective stress (σ_z') and strain (ε_z). Figs. 9(b) and 9(c) are related to horizontal effective stress (σ_x', σ_y') and strain ($\varepsilon_x, \varepsilon_y$). It was found that vertical effective stress (σ_z') rapidly increased after loading and became constant after a decrease. It was also confirmed that the strain (ε_z) rapidly increased after loading and decreased and then became constant over time.

In the case of horizontal effective stress (σ_x', σ_y') and strain ($\varepsilon_x, \varepsilon_y$), effective stress rapidly increased by loading and increased after a decrease and then becomes constant. It was also confirmed that the strain was gradually increased after loading, and then the increment was decreased over time. Here, the decrease in effective stress was due to the temporary expansion of sand under the effect of dilatancy.

Fig. 10 shows the calculated contours of vertical effective stress for clay layer (Ma12-1) in three dimensions. Fig. 10(a) indicates calculated contours of vertical effective stress in entire clay layers. Fig. 10(c) is a cut of Fig. 10(a) in the y direction, and Figs. 11(b) and 11(d) are enlargement of the center of Figs. 10(a) and 10(c), respectively. Through the newly developed three-dimensional program, it was easy to see the distribution of calculated contours of vertical effective stress in the clay layers, as shown in these Figures.

Fig. 11 shows the time-effective stress relation and the time-strain relation for a center element of the clay layer

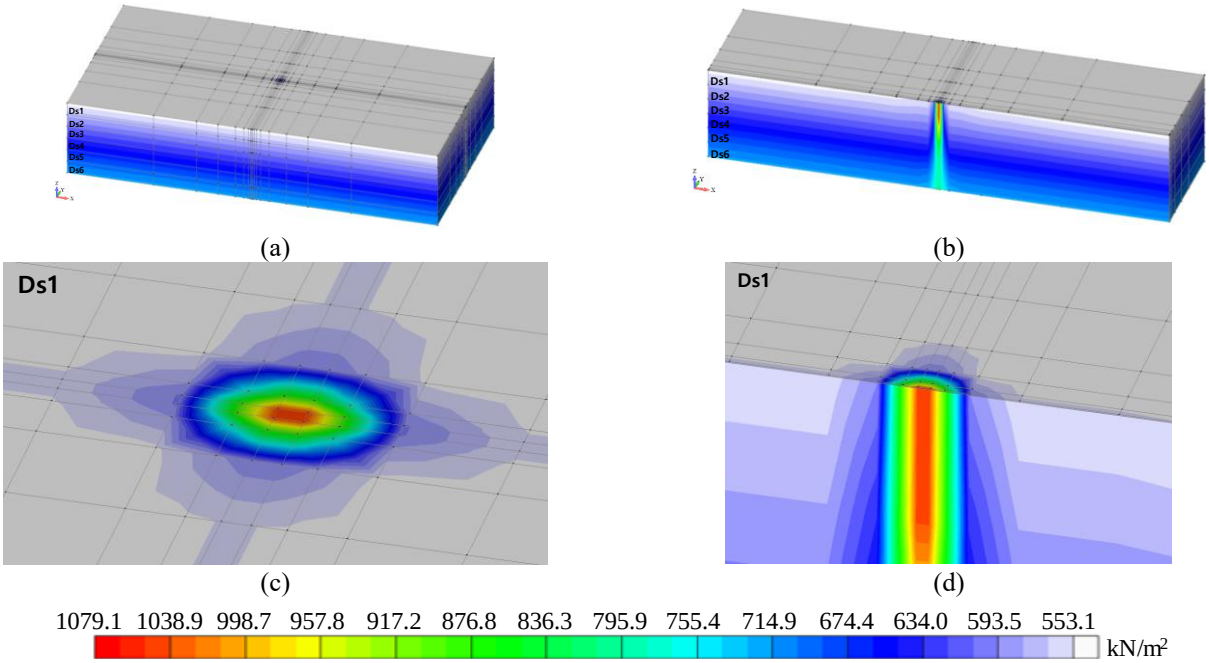

Fig. 8 Calculated contours of vertical effective stress in sand layers

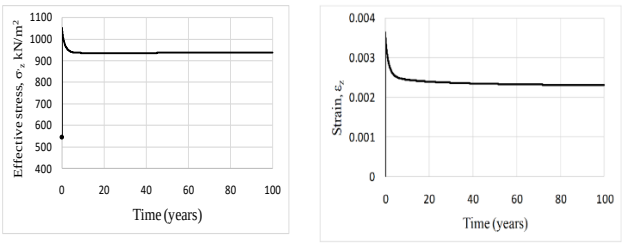

(a) Vertical effective stress(σ_z') and strain(εz)- time relations for sand layer

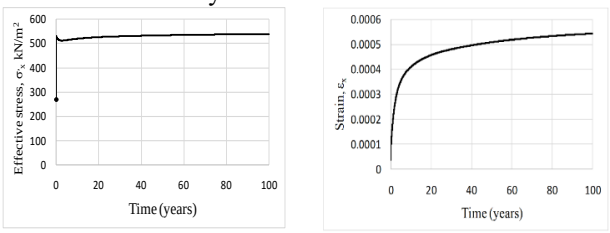

(b) Horizontal effective stress(σ_x') and strain(εx)- time relations for sand layer in x direction

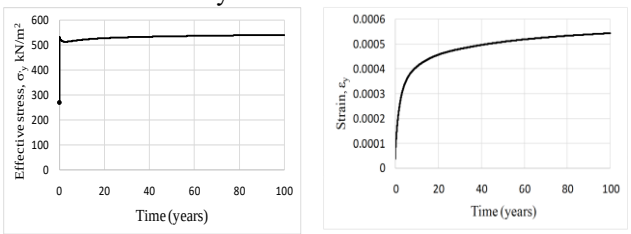

(c) Horizontal effective stress(σ_y') and strain(εy)- time relations for sand layer in y direction

Fig. 9 Calculated effective stress and strain- time relations for sand layer

(Ma12-1). Fig. 11(a) is related to vertical effective stress (σ_z') and strain (ε_z). Figs. 11(b) and 11(c) are related to horizontal effective stress (σ_x', σ_y') and strain ($\varepsilon_x, \varepsilon_y$). It was found in Fig. 11(a) that vertical effective stress (σ_z') rapidly increased after loading and decreased gradually. It was also confirmed that the strain (ε_z) was gradually increased after loading, and then the increment was decreased over time.

In the case of horizontal effective stress (σ_x', σ_y') and strain ($\varepsilon_x, \varepsilon_y$), effective stress gradually increased after loading, and then the increment decreased over time. It was also confirmed that the strain was gradually increased after loading. However, unlike strain ($\varepsilon_x, \varepsilon_y$) of the sand layer, the clay layer strain ($\varepsilon_x, \varepsilon_y$) represents expansion as a (-) sign. In this study, strain was expressed according to the geotechnical engineering convention, where compressive strain is taken as positive and expansive strain as negative.

Fig. 12 shows the relation of $\Delta\sigma_z'/\sigma_{zo}'$ with depth in the center element of each layer, and Fig. 13 show the relation of $\Delta\sigma_z'/\sigma_{zo}'$ with wide. These results can only be known through three-dimensional analysis. The $\Delta\sigma_z'/\sigma_{zo}'$ was greatest at Ds1, where the load was applied directly and then decreased with increasing depth. In the case of the relation of $\Delta\sigma_z'/\sigma_{zo}'$ with wide, it was a natural result. The $\Delta\sigma_z'/\sigma_{zo}'$ in the sand with large effects of the load appeared more than in the clay. However, the range of effects of stress appeared to be wider in the clay layer.

3.3 Performance of settlement, horizontal displacement and deformation

Fig. 14 shows the results for settlement. Here, the settlement of each layer is the average value related to the upper four nodes in the uppermost element of each layer. Fig. 14(a) shows the time-settlement relations of the sand layer. As soon as the loading was applied, immediate settlement appeared and then remained constant. Fig. 14(b)

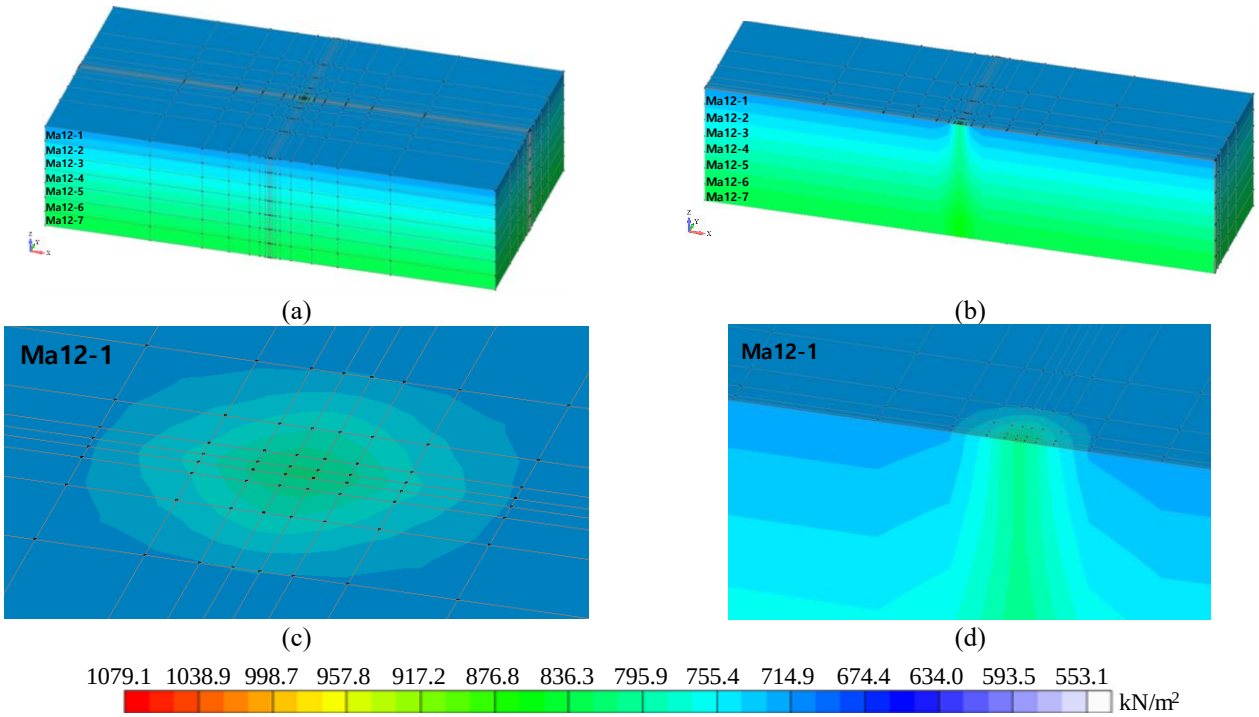

Fig. 10 Calculated contours of vertical effective stress in clay layers

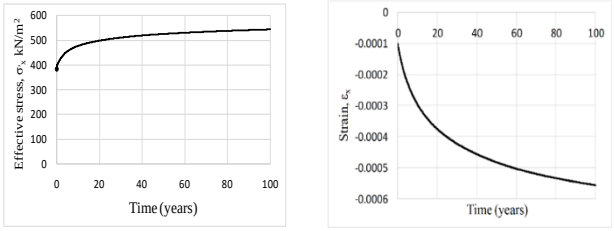

(a) Vertical effective stress(σ_z') and strain(εz)- time relations for clay layer

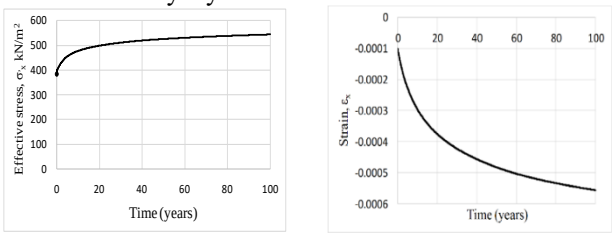

(b) Horizontal effective stress(σ_x') and strain(εx)- time relations for clay layer in x direction

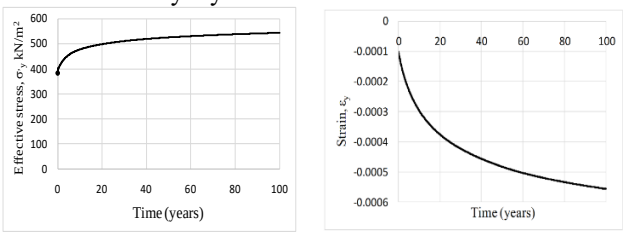

(c) Horizontal effective stress(σ_y') and strain(εy)- time relations for clay layer in y direction

Fig. 11 Calculated effective stress and strain- time relations for clay layer

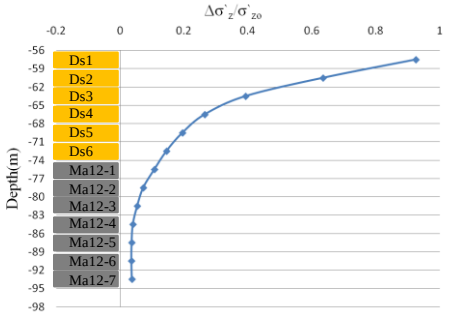

Fig. 12 Relation of $\Delta\sigma_z'/\sigma_{zo}'$– depth

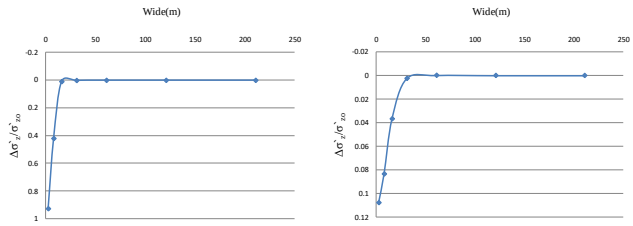

Fig. 13 Relation of $\Delta\sigma_z'/\sigma_{zo}'$– wide

shows the time-settlement relations of the clay layer. The clay layer also appeared with a little immediate settlement. After that, settlement proceeded with time in accordance with characteristics of quasi-over-consolidation without consolidation yield. Even after 100 years, the settlement is still ongoing. As shown in Fig. 14(c), the total settlement appeared to be about 9.9 cm after 100 years.

Figs. 15 and 16 show the result of horizontal displacement for a center element of the sand layer (Ds1) and clay layer (Ma12-1), respectively. Figs. 15(a) and 16(a)

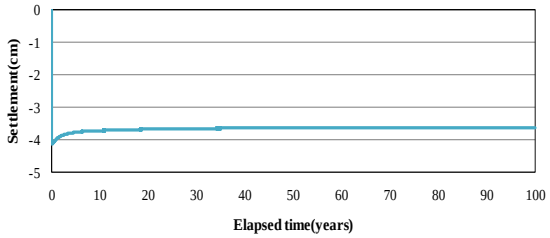

(a) Time-settlement relations of the sand layer

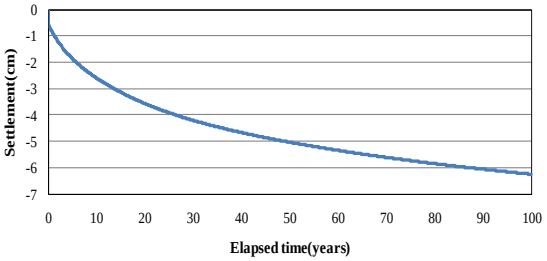

(b) Time-settlement relations of the clay layer

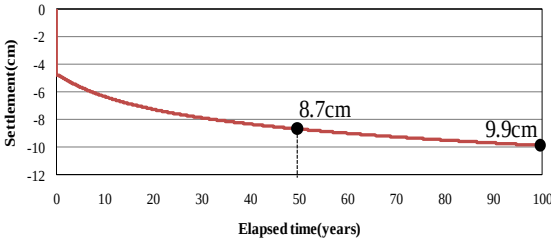

(c)= (a)+(b)

Fig. 14 Calculated displacement - time relation

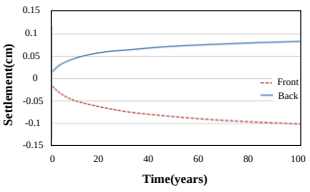

(a) Horizontal displacement in x direction

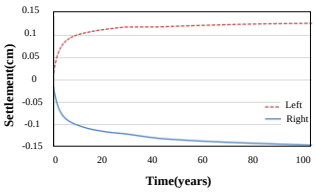

(b) Horizontal displacement in y direction

Fig. 15 Calculated horizontal displacement - time relations for element of sand layer(Ds1)

shows the horizontal displacement in the x direction. Here, "left" is the average value for the left side of the four nodes, and "right" is the average value for the right side of the four nodes. Figs. 15(b) and 16(b) shows the horizontal displacement in y direction. Here, "front" is the average value for the front side of four nodes, and "back" is the average value for the back side of four nodes.

It was confirmed that the actual shape of the deformation for a center element of sand and clay layer in Fig. 17 well explained these results of settlement and horizontal displacement. In the case of the sand layer, $\varepsilon_x, \varepsilon_y, \varepsilon_z$ showed compressive deformation, and volumetric strain (ε_v) also took place compressive deformation. In the case of clay, volumetric strain (ε_v) also appeared to have compressive deformation, but the aspect differed from the sand layer. $\varepsilon_x, \varepsilon_y$ indicated expanded deformation. Nevertheless, volumetric strain still appeared to have compressive deformation.

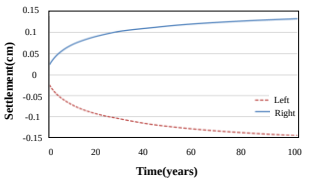

(a) Horizontal displacement in x direction

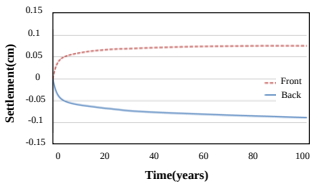

(b) Horizontal displacement in y direction

Fig. 16 Calculated horizontal displacement - time relations for element of clay layer(Ma12-1)

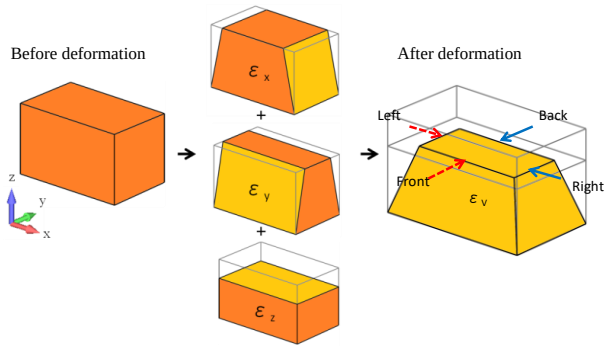

(a) Deformation of a center element for sand layer(Ds-1)

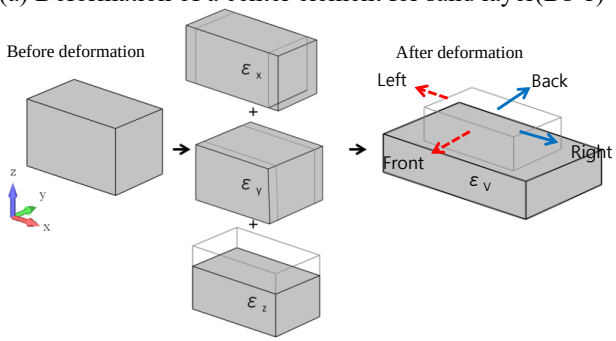

(b) Deformation of a center element for clay layer(Ma12-1)

Fig. 17 Deformation of a central element

4. Conclusions

In this study, a three-dimensional elasto-viscoplastic finite element analysis was conducted to investigate the stress and deformation behavior of Pleistocene foundations subjected to locally applied loading from a pile-supported elevated bridge. The key findings are summarized as follows:

1. The developed three-dimensional model effectively captured the stress dispersion characteristics and revealed a significant reduction in stress increment with depth beneath the loaded area. This redistribution behavior could not be simulated using conventional two-dimensional approaches, highlighting the importance of 3D analysis in complex subsurface conditions.

2. The settlement of the Pleistocene clay layers was predicted to remain within 10 cm over a 100-year period, including approximately 5 cm of immediate settlement followed by long-term creep. These results indicate the stable long-term performance of the pile-supported foundation system on Pleistocene marine deposits.

3. The deformation pattern was characterized by dominant vertical compression accompanied by lateral expansion in the clay layers. The model successfully reproduced the time-dependent behavior of quasi-overconsolidated clay subjected to sustained loading.

4. From a practical standpoint, the results of this study offer useful design insights for pile-supported structures constructed on heterogeneous Pleistocene ground, particularly in reclaimed coastal areas where stratification irregularities and permeability variations are common.

5. Future studies may include parametric analyses considering pile spacing, pile cap rigidity, and alternative loading conditions to further extend the applicability of the proposed framework. The potential integration of field monitoring data could also assist in the calibration and validation of model parameters.

Overall, this study demonstrates that a three-dimensional analysis approach is essential for realistically assessing the stress and deformation behavior of piled foundations under localized loading and provides a valuable reference for future geotechnical design in soft reclaimed ground.

Acknowledgments

This research was supported by Basic Science Research Program through the National Research Foundation of Korea (NRF) funded by the Ministry of Education (No. 2022R1I1A1A01073509).

References

Akai, K. and Tamura, T. (1976), "An application of nonlinear stress-strain relations to multi-dimensional consolidation problems", *Annuals DPRI, Kyoto University*, **21**(2), 19-35.

Christian, J.T. (1968), "Undrained stress distribution by numerical method", *J. Soil Mech. Found. Div. ASCE*, **94**(6), 1333-1345. https://doi.org/10.1061/JSFEAQ.0001199.

Ito, Y., Takemura, K., Kawabata, D., Tanaka, Y. and Nakaseko, K. (2001), "Quaternary tectonic warping and strata formation in the Southern Osaka Basin inferred from reflection seismic interpretation and borehole sequences", *J. Asian Earth Sci.*, **20**(1), 45-58. https://doi.org/10.1016/S1367-9120 (01)00019-0.

Jeon, B.G. (2012), "Numerical assessment for long-term behavior of the pleistocene marine foundations due to construction of large-scale offshore airport fill", Ph.D. Dissertation, University of Kyoto, Japan.

Jeon, B.G. and Mimura, M. (2011), "Interactive behavior of the pleistocene reclaimed foundations due to the construction of the adjacent reclamation", *Disaster Prev. Res. Inst., Kyoto Univ.*, **54**, 247-262. http://ci.nii.ac.jp/naid/120003551108.

Kobayashi, G., Mitamura, M. and Yoshikawa, S. (2001), "Lithofacies and sedimentation rate of Quaternary sediments from deep drilling cores in the Kobe area", Southwest Japan, *Earth Sci.*, **55**, 131-143. https://doi.org/10.15080/agcjchikyukagaku.55.3_131.

Mimura, M. and Jang, W.Y. (2004), "Description of time-dependent behavior of quasi-overconsolidated Osaka Pleistocene clays using elasto-viscoplastic finite element analyses", *Soils Found.*, **44**(4), 41-52. https://doi.org/10.3208/sandf.44.4_41.

Mimura, M. and Jeon, B.G. (2011), "Numerical assessment for the behavior of the Pleistocene marine foundations due to construction of the 1st phase Island of Kansai International Airport", *Soils Found.*, **51**(6), 1115-1128. https://doi.org/10.3208/sandf.51.1115.

Mimura, M. and Jeon, B.G. (2013), "Interactive behavior of Pleistocene marine foundation of existing 1st phase island due to construction of 2nd phase island of Kansai International Airport", *Soil Found.*, **53**(3), 375-394. https://doi.org/10.1016/j.sandf.2013.04.001.

Mimura, M. and Sekiguchi, H. (1986), "Bearing capacity and plastic flow of rate-sensitive clay under strip loading", *Bull. Disaster Prevent. Res. Inst.*, **36**(2), 99-111. https://api.semanticscholar.org/CorpusID:67848789.

Nawel, B. and Salah, M. (2015), "Numerical modeling of two parallel tunnels interaction using three-dimensional Finite Elements Method", *Geomech. Eng.*, **9**(6), 775-791. https://doi.org/10.12989/gae.2015.9.6.775.

Sekiguchi, H. (1977), "Rheological characteristics of clays", *Proceedings of the 9th International Conference on Soil Mechanics and Foundation Engineering*, Tokyo, July

Song, F. and Tian, Y. (2019), "Three-dimensional numerical modelling of geocell reinforced soils and its practical application", *Geomech. Eng.*, **17**(1), 1-9. https://doi.org/10.12989/gae.2019.17.1.001.

Sun, W., Xue, Y., Yin, L. and Zhang, J. (2019), "Experimental study on seepage characteristics of large size rock specimens under three-dimensional stress", *Geomech. Eng.*, **18**(6), 567-574. https://doi.org/10.12989/gae.2019.18.6.567.

Wikipedia (2009), Osaka Bay; Wikipedia. https://en.wikipedia.org/wiki?curid=378451.

Yamaguchi, K., Takeuchi, N. and Hamasaki, E. (2018), "Three-dimensional simplified slope stability analysis by hybrid-type penalty method", *Geomech. Eng.*, **15**(4), 947-955. https://doi.org/10.12989/gae.2018.15.4.947.

Yang, X.L. and Liu, Z.A. (2018), "Reliability analysis of three-dimensional rock slope", *Geomech. Eng.*, **15**(6), 1183-1191. https://doi.org/10.12989/gae.2018.15.6.1183.

Yun, S.K. (2020), "Demonstration of developed numerical procedure to describe 3-dimensional long-term behavior of the Pleistocene marine foundations", *J. Korean Geotech. Soc.*, **36**(7), 5-14. https://doi.org/10.7843/kgs.2020.36.7.5.

IC